ISSN 1990-7931, Russian Journal of Physical Chemistry B, 2025, Vol. 19, No. 4, pp. 783–791. © Pleiades Publishing, Ltd., 2025.

STRUCTURE OF CHEMICAL COMPOUNDS, QUANTUM CHEMISTRY, SPECTROSCOPY

Magnetic, Optical and Thermoelectric Properties of EuGaN for Next-Generation Energy and Electronic Tehcnologies

B. Bouabdallah[a], B. Amiri[b], A. Nouri[a], K. Bouferrache[c, d], M. A. Ghebouli[c, e], M. Fatmi[c, *], B. Ghebouli[f], and F. K. Alanazi[g, **]

[a] *Laboratory for the Development of Renewable Energies and Their Applications in Saharan Areas (LDREAS), Faculty of Exact Sciences, TAHRI Mohammed University, BP 417, Bechar, 08000 Algeria*

[b] *Higher Normal School of Bechar, Bechar, 08000 Algeria*

[c] *Research Unit on Emerging Materials (RUEM), University Ferhat Abbas of Setif 1, Setif, 19000 Algeria*

[d] *Department of Physics, Faculty of Sciences, University of Mohamed Boudiaf, M'Sila, 28000 Algeria*

[e] *Department of Chemistry, Faculty of Sciences, University of Mohamed Boudiaf, M'Sila, 28000 Algeria*

[f] *Laboratory for the Study of Surfaces and Interfaces of Solid Materials (LESIMS), University Ferhat Abbas of Setif 1, Setif, 19000 Algeria*

[g] *Department of Physics, college of Sciences, Northern Border University, P.O. Box 1321, Arar, 91431 Saudi Arabia*

**e-mail: fatmimessaoud@yahoo.fr*

***e-mail: Faisal.katib.al@gmail.com*

Received February 27, 2025; revised March 14, 2025; accepted March 20, 2025

Abstract—This study explores the Magnetic, Optical and thermoelectric properties of europium-doped Gallium Nitride (Eu:GaN) using the Full-Potential Linearized Augmented Plane Wave method within Density Functional Theory framework, employing the Modified Becke–Johnson method. By substituting a Gallium atom with a Europium atom in the hexagonal crystal structure of GaN with a nominal doping rate of 6%, characteristic electronic transitions and localized magnetic moments associated with Eu^{3+} ions were revealed through our calculations. Additionally, optical analysis revealed enhanced Absorption, particularly in the Ultraviolet region, while thermoelectric properties, calculated using the Boltz-TraP program, demonstrated significant enhancements in electrical conductivity and Power Factor up to 800 K. The figure of Merit reached 0.955 at room temperature. These findings highlight the potential of EuGaN for a range of applications, including use in optoelectronics such as ultraviolet detectors, LEDs and ultraviolet photovoltaics, as well as in thermoelectric devices such as waste heat recovery and thermoelectric generators. This paves the way for future research on rare earth-doped materials.

Keywords: EuGaN, DFT, optical properties, thermoelectrics, WIEN2K, mBJ+U

DOI: 10.1134/S1990793125700484

1. INTRODUCTION

Semiconductor based devices have been extensively utilized in a myriad of domains, encompassing Microelectronics, optoelectronic devices, and chemical sensors [1–3]. Historically, scholarly focus has predominantly been directed towards elemental semiconductors such as Silicon (Si) and Germanium(Ge) [4], alongside conventional III–V semiconductors like Gallium Arsenide (GaAs) and Indium Phosphate (InP) [5]; however, recent studies have explored the intricate properties of nitride semiconductors, including Indium Nitride (InN), Gallium Nitride (GaN), and Aluminum Nitride (AlN) [6], as well as their respective alloys [7–9]. The methodical incorporation of rare earth (RE) doping into nitride semiconductors offers a promising approach to developing advanced visible light- emitting optoelectronic devices [10–12]. Significantly, GaN semiconductors have become pivotal subjects of academic inquiry and technological advancement [13], distinguished by their Wide–Band–Gap characteristics and exceptional mechanical resilience [14–16]. Group III–V semiconductors, such as GaN, InN, and AlN, are instrumental in microelectronic devices functioning in extreme environmental conditions due to their outstanding thermal and electrical properties [17]. The incorporation of RE doping imparts unique attributes to III–V nitrides, thereby affecting their optical and electronic characteristics [18]. For example, the introduction of Eu doping in GaN facilitates the fabrication of red light-emitting devices, offering alternatives to traditional methodologies [19–21].

M. Lantri et al. identified that ErGaN exhibits pronounced UV emission peaks within the range of 99.2

to 198.4 nm. Furthermore, the computed magnetic moments were approximately 3.00 μB across all experimental evaluations [22]. S. Amiri et al. ascertained that ErGaN functions as a semiconductor with an indirect band gap of 0.79 eV, whereas $Eu_{0.06}Ga_{0.94}N$ demonstrated an indirect Band Gap of 3.38 eV utilizing Generalized Gradient Approximation (GGA + U) methodologies [23], corroborating findings from prior investigations [24–26]. This study investigates the potential of EuGaN as a promising material for optoelectronic and thermoelectric Applications. By employing advanced Computational Techniques; the Tran–Blaha modified Becke–Johnson potential with on-site Coulomb repulsion (TB-mBJ + U) methodology, we explore the Electronic, Magnetic, Optical, and Transport Properties of EuGaN. Our aim is to elucidate the impact of Eu doping on GaN's semiconductor behaviors and to identify strategies for enhancing its optical efficiency and electrical conductivity. This paper commences with a thorough exposition of the Computational Methodology, offering a detailed elucidation of the techniques utilized. Subsequent sections delve into an exploration of the electronic properties, band structures, and density of states (DOS) of $Eu_{0.06}Ga_{0.94}N$. A comprehensive analysis of the material's optical and transport characteristics follows. The manuscript concludes with a presentation of the principal findings and a discussion of their ramifications. This work has potential applications in optoelectronics (UV LEDs, UV photodetectors, and UV photovoltaics) due to its enhanced optical absorption. Its thermoelectric properties make it suitable for waste heat recovery, thermoelectric generators (TEGs), and temperature sensors. Additionally, EuGaN could be used in high-performance electronic and spintronic devices, benefiting from its improved electrical and magnetic characteristics. These findings position EuGaN as a promising material for next-generation energy and electronic technologies.

2. COMPUTATIONAL METHODS

The DFT calculations within the GGA [27, 28] framework were performed using the WIEN2k software package [29, 30] and the Perdew–Burke–Ernzerhof (PBE) functional [31]. This computational approach has demonstrated efficacy in predicting structural, electronic, and optical properties of materials exhibiting metallic, ionic, and covalent bonding. To enhance the accuracy of electronic structure calculations, particularly for materials with significant band gaps or strong electron correlations, the mBJ+U method [32, 33] was employed to treat the exchange-correlation potential [34]. This method incorporates the mBJ approximation and a Hubbard U parameter of 8.506 eV and *J* parameter of 1.109 eV for Eu 4*f* electrons, as reported by Lambrecht et al. [35]. This amalgamation improves the precision of electronic structure calculations by better capturing the effects of electronic correlation and electron-electron interactions. A 2 × 2 × 1 supercell containing 32 atoms was used based on the wz-GaN structure [36]. To introduce Eu doping at a concentration of 6%, one Ga atom was substituted with an Eu atom, resulting in the $Eu_{0.06}Ga_{0.94}N$ composition. The use of supercells is a standard approach in DFT-based simulations of doped systems. The Brillouin zone was sampled using a Monkhorst–Pack *k*-point grid with a density of approximately 12 points per angstrom. An energy cutoff of 150 Hartree was adopted for the plane wave basis set. Furthermore, calculations of magnetic properties are performed by taking into acout the spin-polarization directions (spin-up and spin-down orientations). Spin-orbit coupling was included through fully relativistic pseudopotentials. The valence states of Eu, N, and Ga were defined accordingly: 4*d*, 4*f*, 5*s*, 5*p*, 5*d*, and 6*s* for Eu; 2*s*, 2*p* for N; and 4*s*, 3*d*, 4*p* for Ga. Plane wave expansions were employed in the interstitial region with a cutoff $K_{max} = 8/R_{MT}$ determined by the smallest muffin tin sphere radius R_{MT}. A total of 500 *k*-points were used for Brillouin zone integrations. The Dielectric function, a crucial parameter for investigating the optical properties of materials, was calculated to describe the linear response of the system to electromagnetic radiation. Thermoelectric properties were determined using the BoltzTraP code [37] based on ab initio data within the framework of semiclassical Boltzmann transport theory under constant relaxation time and rigid band approximations.

3. DISCUSSION AND DISCUSSION

3.1. Electronic Properties

This study investigates the structural, optical, magnetic, and electronic properties of EuGaN through computational simulation. The substitution of a Ga atom with Eu in the GaN lattice, resulting in $Eu_{0.06}Ga_{0.94}N$, induced structural modifications characterized by an elongated equilibrium lattice constant (Fig. 1). Previous research by H. Sekiguchi et al. emphasized the significant influence of growth temperature on nanocolumn configuration within EuGaN, with higher temperatures promoting lateral growth and lower temperatures favoring independent nanocolumn formation [38].

To elucidate the band structure characteristics, total density of states (TDOS) analyses were conducted. These calculations provide insights into the distribution of electronic states and their occupations. The density of states is a fundamental parameter in band theory calculations [39–41]. Figure 2 presents the calculated band structure and TDOS of $Eu_{0.06}Ga_{0.94}N$ using the mBJ + U approximation, highlighting high-symmetry points in the Brillouin zone [42, 43]. The energy range from −7 to 8 eV effectively captures the Electronic Band Structure, revealing an indirect Band Gap of 2.89 eV, indicative of the material's semiconductor

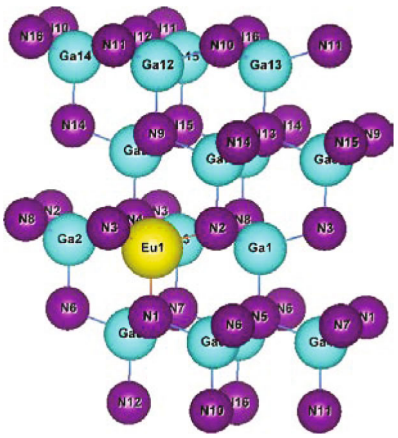

Fig. 1. Crystal structure of $EuGa_{15}N_{16}$.

behavior. Notably, the DOS trends exhibit similarity within this energy range. A high density of states is observed in the valence band between −5 and −1.5 eV, suggesting a substantial number of available electronic states. Conversely, the conduction band displays a significant DOS from 2.89 to 8 eV, indicating ample electronic states for potential transitions from the Valence Band.

An analysis of the electronic properties, summarized in Table 1, provides valuable insights into the material's behavior under different exchange-correlation potentials. Under the local density approximation (LDA), the material exhibits a zero band gap (0.0 eV), suggesting metallic characteristics. However, the calculated total energy (−81671.746 Ry) is relatively low, indicating potential limitations in the LDA model's accuracy. In contrast, the mBJ potential predicts a band gap of 1.027 eV, suggesting a transition towards semiconductor or insulating behavior. The slight increase in total energy compared to the LDA calculation (−81667.064 Ry) supports the mBJ potential's improved representation of the system's total energy. It is well established that different computational methods yield varying Band Gap values for different materials Table 1. The calculated band gap progressively increases from LDA to mBJ to mBJ + U, emphasizing the impact of exchange-correlation potentials on electronic structure. A comparison of optimized and experimental band gaps for GaN and $Eu_{0.06}Ga_{0.94}N$ using the mBJ method is presented in Table 1.

The employment of the mBJ + U potential results in a wider band Gap of 2.898 eV, confirming the insulating nature of the material. While the total energy remains comparable to the mBJ result, a slight decrease (−81666.945 Ry) suggests additional system stabilization. The incorporation of Eu ions introduces localized magnetic moments arising from unpaired 4f electrons of Eu^{3+} ions, influencing the magnetic properties of $Eu_{0.06}Ga_{0.94}N$ [44, 46–48]. Experimental studies by M. Peres et al. reported a Band Gap energy of approximately 1.99 eV for this material [49].

3.2. Optical Properties and Dielectric Function

The electronic properties of solids strongly influence their optical properties. The study of the optical properties of crystals allows us to better understand the

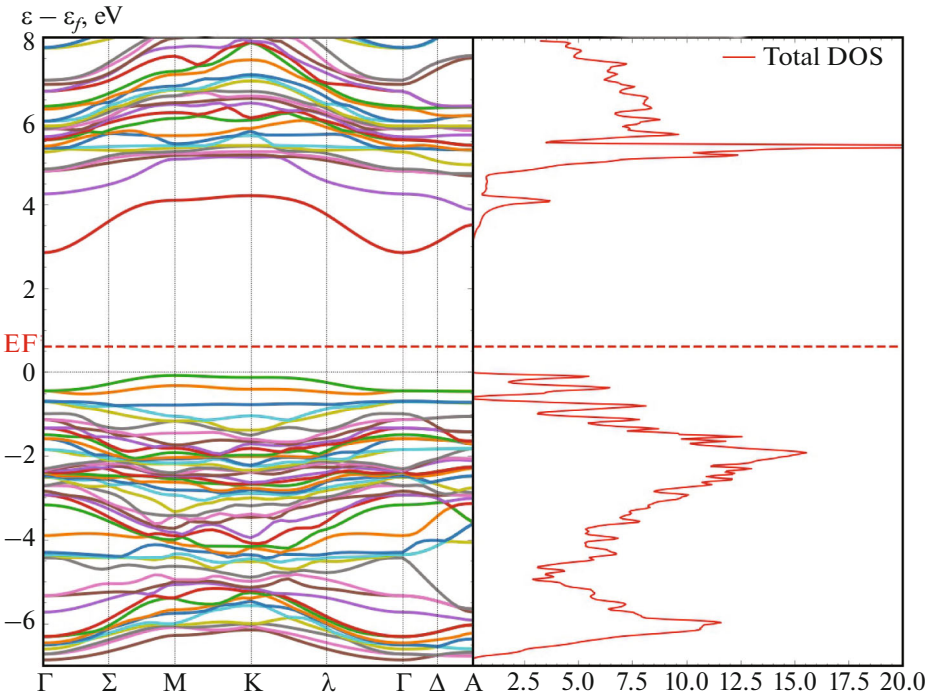

Fig. 2. Band structure and density of states of $Eu_{0.06}Ga_{0.94}N$ material.

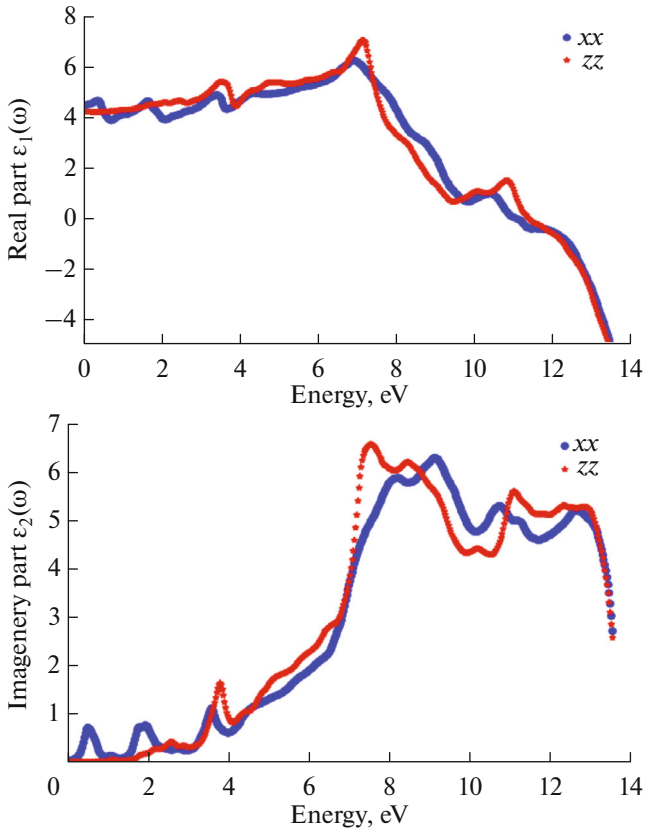

Fig. 3. The real $\varepsilon_1(\omega)$ and imaginary $\varepsilon_2(\omega)$ parts of the dielectric function of $Eu_{0.06}Ga_{0.94}N$.

nature of their response to the frequency of incident photons and to select materials for building optoelectronic devices based on these properties. The frequency-dependent complex dielectric function mainly determines the optical properties of the material [50, 51]. Consequently, the optical absorption, reflection, and transmission coefficients for $Eu_{0.06}Ga_{0.94}N$ are calculated. The optical properties of the material are described by the transverse dielectric function in the following equations [52, 53].

$$\varepsilon(\omega) = \varepsilon_1(\omega) + i\varepsilon_2(\omega), \quad (1)$$

where ω represents the frequency parameter, the dielectric function is a complex quantity that describes how a material responds to electromagnetic radiation. The real part $\epsilon_1(\omega)$, is related to the polarizability of the material, and the imaginary part $\epsilon_2(\omega)$, is related to the absorption of light. The real part of the dielectric function $\epsilon(\omega)$ can be calculated by the Kramers–Kronig transformation [54]:

$$\varepsilon_1(\omega) = 1 + \frac{2}{\pi} P \int_0^{\infty} \frac{\varepsilon_2(\omega')}{\omega'^2 - \omega^2} d\omega', \quad (2)$$

where P represents the Cauchy principal value of the integral. Several peaks are observed in the real and imaginary parts of the dielectric function. In the $\varepsilon_1(\omega)$, the peaks were located at 0.5, 2.5, 3.9 eV and the highest peak was at 7.5 eV. In the $\varepsilon_2(\omega)$, the peaks were at 0.5, 1.9, 3.9 eV and the highest peak was at 7.9 eV. These observations are summarized in Fig. 3.

These peaks indicate different electronic transitions in the material. Low-energy transitions correspond to excitation between valence and conduction band states, conversely, high-energy transitions reflect significant electronic excitations or intraband transitions. These characterization results offer valuable insights into the optical and electronic properties, deepening our understanding of their behaviors in various applications, such as optoelectronics and photovoltaic. Figire 4 displays the results of the optical conductivity σ_{op} and the absorption coefficient $\alpha(\omega)$.

The optical conductivity σ_{op} is essentially the optical response of the material, by analyzing the optical conductivity spectrum, scientists can gain insights into the behaviour of electrons and photons in the material, which is crucial for understanding its optical and electrical properties. The optical conductivity of a polarized medium is found to be governed by:

$$\sigma_{op} = \frac{c\chi}{3\lambda}, \quad (3)$$

where χ is the electric susceptibility. The absorption coefficient α is defined with

$$\alpha = 4\frac{\pi\sigma_{op}}{nc}, \quad (4)$$

where n is the refractive index, Table 2 shows the correlation between the optical conductivity and absorption coefficient.

Table 1. The electronic and magnetic properties of GaN and $Eu_{0.06}Ga_{0.94}N$ materials

Property	Our calculation			Other calculation	
	LDA	mBJ	mBJ + U	mBJ(GaN)	mBJ(EuGaN)
Band gap, eV	0.0	1.027	2.898	3.3 [44]	3.013 [44]
Total energy, Ry	−81671.746	−81667.064	−81666.945	−63860.043 [44]	−81667.302 [44]
Fermi energy, eV	0.608	0.736	0.612	–	–
Spin magnetic moment	6.01286	6.00061	6.00045	–	–
Experimental gap, eV	–	–	–	3.5 [45]	–

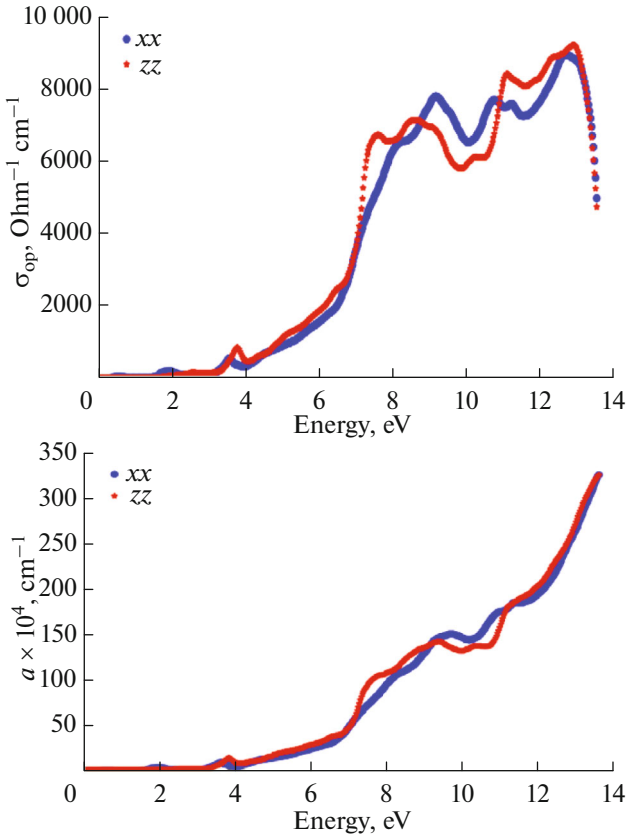

Fig. 4. The optical conductivity and the absorption coefficient of $Eu_{0.06}Ga_{0.94}N$.

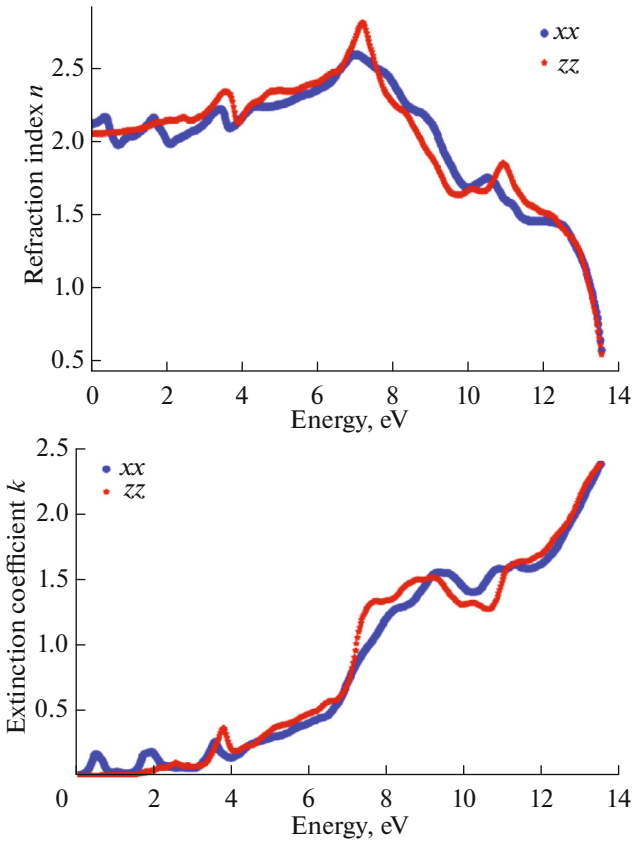

Fig. 5. The refractive index n and extinction coefficient k of $Eu_{0.06}Ga_{0.94}N$.

Table 2 showcases a range of energy from 2.0 to 13.0 eV alongside corresponding to the optical conductivity peaks values. Notably, the conductivity starts to increase and reaches a maximum at 13.0 eV for both directions. The absorption coefficient exhibits a sharp rise at 2.95 eV (420 nm) and then increases exponentially from 4 eV (309.9 nm) towards higher energies. This behavior covers a significant portion of the solar spectrum, with a particularly strong enhancement in the ultraviolet region.

3.3. The Refractive Index and the Extinction Coefficient

The calculated refractive index $n(\omega)$ and extinction coefficient $k(\omega)$ for majority and minority spin are shown in Fig. 5. The complex refractive index $N(\omega)$ is expressed as:

$$N(\omega) = n(\omega) + ik(\omega). \quad (5)$$

It is indicated that the real part of the $n(\omega)$, aligns with the real part of the dielectric function spectrum $\varepsilon_1(\omega)$, while the results of the extinction coefficient $k(\omega)$, correlate well with the imaginary part of the dielectric function $\varepsilon_2(\omega)$.

Figure 5 shows the static refractive index for the *xx* and *zz* directions, with values of 2.1 and 2.2, respectively. The refractive index exhibits an initial increase, reaching a maximum value of 3.0 eV for both directions. Additionally, the extinction coefficient k, starts

Table 2. Summary of optical conductivity and absorption coefficient peaks of $Eu_{0.06}Ga_{0.94}N$

Energy, eV	σ_{op}, Ohm^{-1} cm^{-1}	Energy, eV	$\alpha \times 10^4$, cm^{-1}	Others
2.0	200	2.0	2	2.1 [44]
3.4	1000	3.9	12.25	10 [44]
6.8	6200	7.9	98	52 [44]
8.7	7200	9.8	148	121 [44]
13.0	9000	11.1	187.5	154 [44]

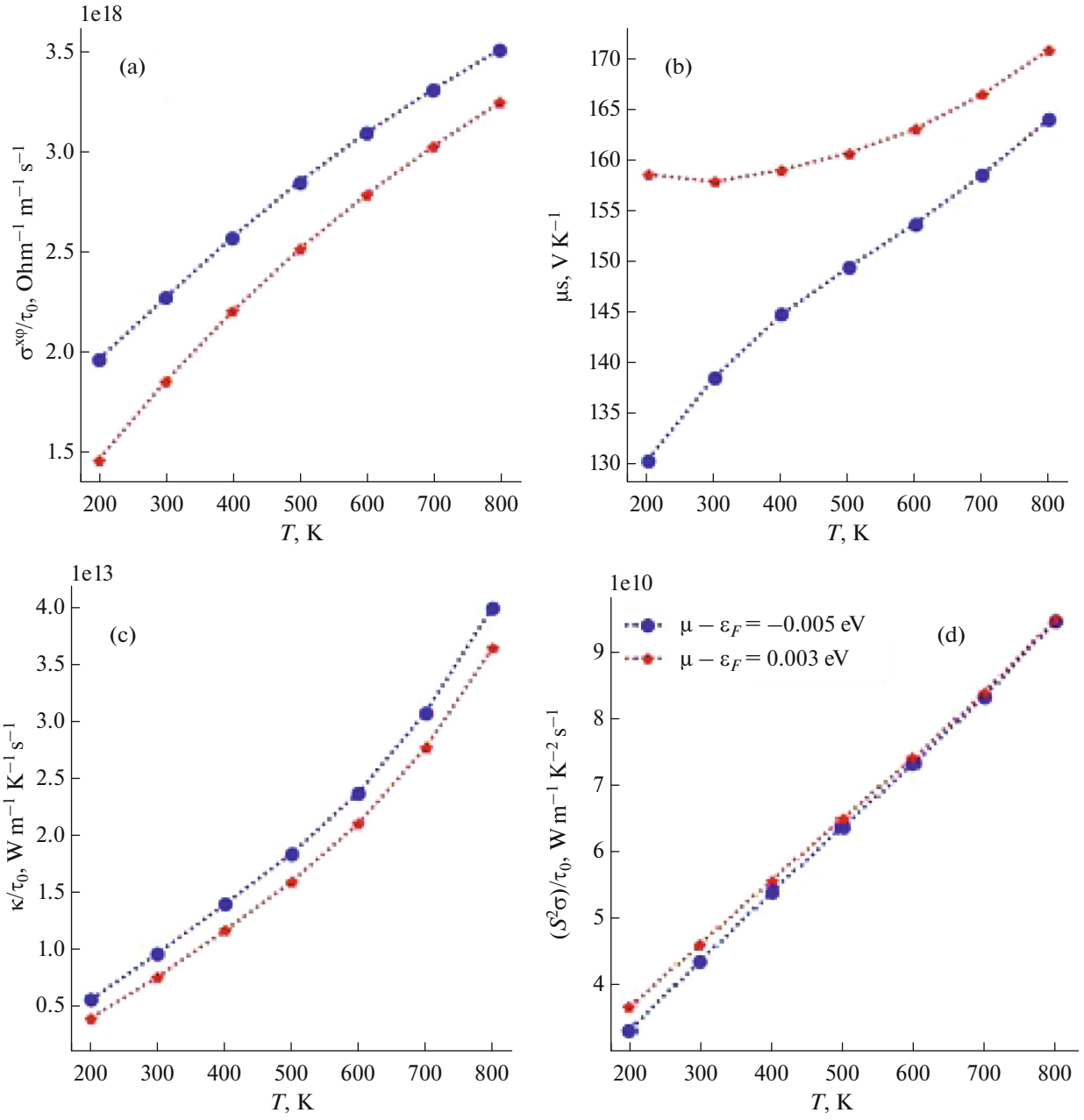

Fig. 6. Temperature dependence of the (a) electrical conductivity, (b) Seebeck coefficient, (c) thermal conductivity, and (d) power factor of $Eu_{0.06}Ga_{0.94}N$.

to increase from 2.0 eV and continues to rise towards higher energies in both *xx* and *zz* directions.

3.4. Transport Properties

To investigate the thermoelectric properties of $Eu_{0.06}Ga_{0.94}N$, we employed the Boltz-TraP program, integrated with WIEN2K, to derive these properties from the Boltzmann semi-classical transport equations [55, 56], A high power factor (PF) and good electrical conductivity are essential for favorable thermoelectric behaviors [57]. Previous studies have highlighted the limitations of GaN in this regard, motivating research to enhance its thermoelectric properties, including electrical conductivity and power factor [58]. We observed a significant increase in σ/τ (Electrical Conductivity divided by Carrier Lifetime) with rising temperature in doped $Eu_{0.06}Ga_{0.94}N$. This enhancement is likely due to the creation of additional energy states near the Fermi level, facilitating increased electron mobility in the conduction band. These additional states are possibly attributed to

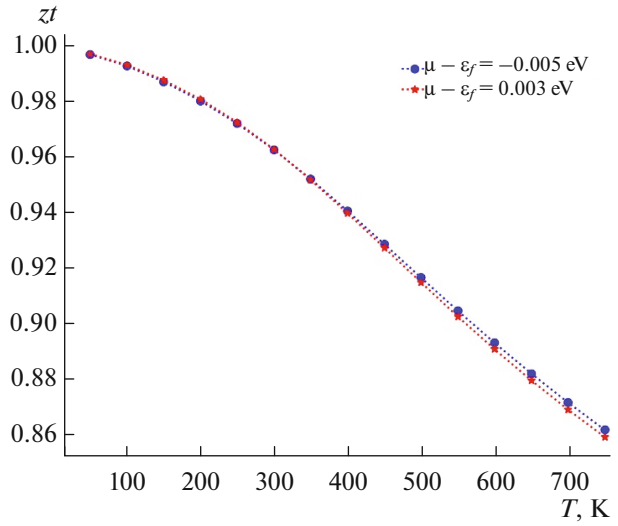

Fig. 7. Figure of Merit ZT of $Eu_{0.06}Ga_{0.94}N$.

impurities from 4*f* states within the conduction band. At higher temperatures, the σ/τ values obtained from our calculations closely match those predicted by the mBJ method [59]. Figure 6 illustrates the temperature dependence of σ/τ for both *p*-type and *n*-type $Eu_{0.06}Ga_{0.94}N$, considering two different chemical potentials such as −0.005 and 0.003 eV. The chemical potential values −0.005 and 0.003 eV are chosen because of their proximity to 0 eV, thus ensuring a relevant comparison in the analysis of transport properties.

As shown in Fig. 6, the electrical conductivity in both n and p regions steadily increases from 200 to 800 K. The n-type material exhibits a slightly higher electrical conductivity, reaching 3.5×10^{18} (Ohm ms)$^{-1}$ compared to 3.25×10^{18} (Ohm ms)$^{-1}$ for the *p*-type material. The Seebeck coefficient for *n*-type and *p*-type regions were calculated to be 163.45 and 170.05 μV/K, respectively, exactly at 800 K. The electronic thermal conductivity (k_e/τ) remains relatively low at room temperature but increases with rising temperature [60, 61]. The power factor, *PF*, is directly proportional to the square of the Seebeck coefficient times the electrical conductivity $PF = S^2(\sigma/\tau)$. At 800 K, the power factor of $Eu_{0.06}Ga_{0.94}N$ for both *n* and *p* types are 9.6×10^{10} W/m K^2 s. Figure 7 presents the temperature-dependent Figure of Merit (ZT) for both *n*- and *p*-type $Eu_{0.06}Ga_{0.94}N$.

The comprehensive study range from 50 to 800 K allows for the evaluation of thermoelectric performance across various temperature regimes. At 100 K (−173.15°C), the focus is on applications in cryogenic cooling and low-temperature waste heat recovery. Conversely, at 800 K, the material's suitability for high-temperature industrial processes is assessed. Our primary interest lies in the thermoelectric performance at room temperature, which is directly relevant to everyday applications. At this temperature, the observed ZT value of 0.955, approaching the ideal ZT of 1, indicates the promising potential of $Eu_{0.06}Ga_{0.94}N$ for Thermoelectric conversion. These findings motivate further research and development to explore its applications in diverse fields, including waste heat recovery, solar thermoelectric systems and space exploration [60].

4. CONCLUSIONS

This study employed the FP-LAPW method within the DFT framework to investigate the Magnetic, optical, and Thermoelectric properties of 6% Eu-doped GaN. The introduction of Eu resulted in the emergence of characteristic electronic transitions and localized magnetic moments associated with Eu^{*+} ions, indicating the possibility of ferromagnetic behaviors. The enhanced optical absorption in the UV region (around 428 nm) positions $Eu_{0.06}Ga_{0.94}N$ as a promising candidate for optoelectronic applications such as UV photovoltaics, LEDs and UV Sensors. It is noteworthy that the material displayed considerable enhancements in electrical conductivity and power factor, thereby confirming its *p*-type semiconductor nature. The calculated figure of merit of 0.955 at at room temperature serves to underscore the potential of this material for use in efficient Thermoelectric Power Generators, Waste Heat Recovery and temperature sensors. These findings collectively indicate that Eu-doped GaN is a versatile material with applications in both optoelectronic and thermoelectric. Further research could investigate the effects of varying Eu doping concentrations and the potential of other rare earth dopants to optimize these properties.

ACKNOWLEDGMENTS

The authors extend their appreciation to the Deanship of Scientific Research at Northern Border University, Arar, KSA for funding this research work through the project no. NBU-FFR-2025-310-04.

AUTHOR CONTRIBUTION

Conceptualization: B. Bouabdallah, A. Nouri.

Formal analysis: B. Amiri, B. Ghebouli.

Methodology, Validation: M. Fatmi, Faisal Katib Alanazi.

Software: K. Bouferrache.

Writing—review and editing: M.A. Ghebouli.

FUNDING

This work was supported by ongoing institutional funding. No additional grants to carry out or direct this particular research were obtained.

DATA AVAILABILITY

Data underlying the results presented in this paper are not publicly available at this time but may be obtained from the corresponding author (fatmimessaud@yahoo.fr) upon reasonable request.

CONFLICT OF INTEREST

The authors of this work declare that they have no conflicts of interest.

REFERENCES

1. P. Xia, Y. Song, Y. Liu, et al., J. Mater. Chem. C **12**, 1609 (2024). https://doi.org/10.1039/D3TC03329E
2. M. N. Boumezrag, K. Almi, S. Lakel, et al., Russ. J. Phys. Chem. B **18**, 895 (2024). https://doi.org/10.1134/S1990793124700325
3. M. A. Ahmed and A. A. Mohamed, RSC Adv. **13** (1) 421 (2023) https://doi.org/10.1039/D2RA07225D
4. F. Murakami, A. Takeo, et al., Commun. Mater. **4** (1) 100 (2023). https://doi.org/10.1038/s43246-023-00428-6
5. R. Moussa, A. Abdiche, R. Khenata, et al., Opt. Mater. **113**, 110850 (2021). https://doi.org/10.1016/j.optmat.2021.110850
6. K. Chinnadurai and B. Natesan, Comput. Condens. Matter **38**, e00871 (2024). https://doi.org/10.1016/j.cocom.2023.e00871
7. J. Wang, L. Liu, and J. Tian, Solid State Commun. **389**, 115587 (2024). https://doi.org/10.1016/j.ssc.2024.115587
8. H. Zhang, C. Huang, K. Song, et al., Rep. Prog. Phys. **84** (4), 044401 (2021). https://doi.org/10.1088/1361-6633/abde93
9. J. Tournet, Y. Lee, S. K. Karuturi et al., ACS Energy Lett. **5** (2) 611–622 (2020). https://doi.org/10.1021/acsenergylett.9b02582
10. J. Zhang and W. Wang, Russ. J. Phys. Chem. B **17**, 293–300 (2023). https://doi.org/10.1134/S1990793123020343
11. M. J. Winiarski, Materials **14** (15), 4115 (2021). https://doi.org/10.3390/ma14154115
12. A. Bendahah, D. Bensaid, A. Yhaia, et al., Emergent Mater. **7**, 2787–2795 (2024). https://doi.org/10.1007/s42247-024-00756-4
13. F. Mollaamin and M. Monajjemi, Russ. J. Phys. Chem. B **18**, 533–548 (2024). https://doi.org/10.1134/S199079312402012X
14. M. S. Wong, E. S. Trageser, and H. Zhang, Opt. Express **32** (12), 20483 (2024). https://doi.org/10.1364/OE.520339
15. P. Kempisty, A. Ahmad, P. Strak, et al., Comput. Mater. Sci. **230**, 112489 (2023). https://doi.org/10.1016/j.commatsci.2023.112489
16. Y. Tang, Z. Ren, Q. Lei, et al., Comput. Mater. Sci. **222**, 112118 (2023). https://doi.org/10.1016/j.commatsci.2023.112118
17. S. Nakamura, M. Senoh, S. Nagahama, et al., Appl. Phys. Lett. **69** (26), 4056–4058 (1996). https://doi.org/10.1063/1.117816
18. T. Kallel, T. Koubaa, M. Dammak, et al., J. Lumin. **134**, 893–899 (2013). https://doi.org/10.1016/j.jlumin.2012.06.021
19. M. Y. Widianto, IOP **1175**, 012090 (2019). https://doi.org/10.1088/1742-6596/1175/1/012090
20. C. Braun, L. Mereacre, Z. Chen, et al., Sci. Rep. **12**, 2503 (2022). https://doi.org/10.1038/s41598-022-06148-0
21. Z. Dridi, A. Lazreg, H. Rozale et al., Comput. Mater. Sci. **48** (4) 743 (2010). https://doi.org/10.1016/j.commatsci.2010.03.025
22. M. Lantri, A. Boukortt, S. Meskine, et al., Mod. Phys. Lett. B **33** (27), 1950327 (2019). https://doi.org/10.1142/S0217984919503275
23. S. Amiris, K. Agroui, B. Amiri, et al., Rev. Mex. Fis. **68** (3), 1–8 (2022). https://doi.org/10.31349/RevMexFis.68.031301
24. E. Maskar, A. F. Lamrani, A. Es-Smairi, et al., Comput. Condens. Matter **38**, e00873 (2024). https://doi.org/10.1016/j.cocom.2023.e00873
25. A. Kourdaci, I. Bourachid, H. Bouafia, et al., Comput. Condens. Matter **38**, e00889 (2024). https://doi.org/10.1016/j.cocom.2024.e00889
26. S. Paliwal, V. Maurya, and K. Joshi, Comput. Condens. Matter **32**, e00715 (2022). https://doi.org/10.1016/j.cocom.2022.e00715
27. H. A. Almodarresiyeh, S. Shahab, S. Kaviani, et al., Russ. J. Phys. Chem. B **17**, 12–26 (2023). https://doi.org/10.1134/S1990793123010165
28. A. Abdelakader, B. Ahmed, M. Noureddine, et al., Solid State Commun. **380**, 115435 (2024). https://doi.org/10.1016/j.ssc.2024.115435
29. I. Asfour, Russ. J. Phys. Chem. B **18**, 83–94 (2024). https://doi.org/10.1134/S1990793124010032
30. P. Blaha, K. Schwarz, F. Tran, et al., J. Chem. Phys. **152** (7) (2020). https://doi.org/10.1063/1.5143061
31. J. P. Perdew, K. Burke, and M. Ernzerhof, "Generalized gradient approximation made simple," Phys. Rev. Lett. **77**, 3865 (1996). https://doi.org/10.1103/PhysRevLett.77.3865
32. K. Kourchid, R. Alaya, N. Bouguila, N., et al., Russ. J. Phys. Chem. B **18**, 37–48 (2024). https://doi.org/10.1134/S1990793124010317
33. G. Kadim, R. Masrour, and A. Jabar, Mater. Today Commun. **26**, 102071 (2021). https://doi.org/10.1016/j.mtcomm.2021.102071
34. G. Rehman, M. Shafiq, Saifullah, et al., J. Electron. Mater. **45**, 3314–3323 (2016). https://doi.org/10.1007/s11664-016-4492-7
35. P. Larson, W. R. Lambrecht, A. Chantis, et al., Condens. Matter Mater. Phys. **75** (4), 045114 (2007). https://doi.org/10.1103/PhysRevB.75.045114
36. F. Roccaforte and M. Leszczynski, *Nitride Semiconductor Technology: Power Electronics and Optoelectronic Devices* (Wiley, 2020), pp. 1–39. https://doi.org/10.1002/9783527825264.ch1

37. G. K. Madsen and D. J. Singh, Comput. Phys. Commun. **175** (1), 67–71 (2006). https://doi.org/10.1016/j.cpc.2006.03.007
38. H. Sekiguchi, S. Nishikawa, and T. Imanishi, Jpn. J. Appl. Phys. **55**, 05FG07 (2016). https://doi.org/10.7567/JJAP55.05FG07
39. V. I. Anisimov, J. Zaanen, and O. K. Andersen, Phys. Rev. B **44** (3), 943 (1991). https://doi.org/10.1103/PhysRevB.44.943
40. K. Habura, M. Afrassa, and F. Hone, Comput. Condens. Matter **35**, e00799 (2023). https://doi.org/10.1016/j.cocom.2023.e00799
41. W. O. Santos, A. M. Rodrigues, E. R. P. de Novais, et al., Comput. Condens. Matter **35**, e00796 (2023). https://doi.org/10.1016/j.cocom.2023.e00796
42. M. A. Rehman, Z. ur Rehman, M. Usman, et al., Solid State Commun. **380**, 115447 (2024). https://doi.org/10.1016/j.ssc.2024.115447
43. X. Xu, W. Zeng, D. Hong, et al., Comput. Condens. Matter **35**, e00792 (2023). https://doi.org/10.1016/j.cocom.2023.e00792
44. E. Maskar, A. Fakhim Lamrani, M. Belaiche, et al., Surf. Interfaces **24**, 101051 (2021) https://doi.org/10.1016/j.surfin.2021.101051
45. O. Madelung, *Semiconductors: Data Handbook* (Springer Science & Business Media, 2004).
46. M. Azmat, J. Yang, Q. Li, et al., Ceram. Int. **50** (7), 11119–11128 (2024). https://doi.org/10.1016/j.ceramint.2024.01.013
47. S. Yudate, R. Sasaki, T. Kataoka, and S. Shirakata, Opt. Mater. **28** (6–7), 742–745 (2006). https://doi.org/10.1016/j.optmat.2005.09.013
48. S. Tian, L. Zhang, R. Xie, A. Lu, et al., Solid State Commun. **371**, 115292 (2023). https://doi.org/10.1016/j.ssc.2023.115292
49. M. Kmichou, R. Masrour, L. Xu, et al., Comput. Mater. Sci. **235**, 112805 (2024). https://doi.org/10.1016/j.commatsci.2024.112805
50. H. T. Mumu, A. Zaman, F. H. Bhuiyan, et al., Micro Nanostruct. **174**, 2 (2023). https://doi.org/10.1016/j.micrna.2022.207470
51. I. E. Fragkos, V. Dierolf, Y. Fujiwara, and N. Tansu, Sci. Rep. **7**, 12 (2017). https://doi.org/10.1038/s41598-017-17033-6
52. M. P. Polak and D. Morgan, Comput. Mater. Sci. **193**, 110281 (2021). https://doi.org/10.1016/j.commatsci.2021.110281
53. G. K. Madsen, J. Carrete, and M. J. Verstraete, Comput. Phys. Commun. **231**, 140–145 (2018). https://doi.org/10.1016/j.cpc.2018.05.007
54. Y. Nouri, B. Hartiti, A. Batan, et al., Solid State Commun. **339**, 114491 (2021). https://doi.org/10.1016/j.ssc.2021.114491
55. B. Hu, W. Bao, G. Chen, et al., Comput. Mater. Sci. **230**, 112485 (2023). https://doi.org/10.1016/j.commatsci.2023.112485
56. B. Ul Haq, S.-H. Kim, and M. Alsardia, Curr. Appl. Phys. **49**, 6–11 (2023). https://doi.org/10.1016/j.cap.2023.02.005
57. A. Reshak, RSC Adv. **5** (42), 33632–33638 (2015). https://doi.org/10.1039/C5RA00746A
58. B. Amiri, A. Lazreg, and F. A. Bensaber, Optik **240**, 166798 (2021). https://doi.org/10.1016/j.ijleo.2021.166798
59. P. M. Gadhavi, K. Sivalertporn, P. Poopanya, and M. Talati, Comput. Condens. Matter **38**, e00875 (2024). https://doi.org/10.1016/j.cocom.2023.e00875
60. J. Wang, C.-H. Chen, R. Bonner, et al., in *AIAA Propulsion and Energy 2019 Forum* (2019), p. 3977. https://doi.org/10.2514/6.2019-3977